Dynamic cortical actin remodeling by ERM proteins controls BCR microcluster organization and integrity

Bebhinn Treanor, David Depoil, Andreas Bruckbauer, and Facundo D. Batista

Lymphocyte Interaction Laboratory, London Research Institute, Cancer Research UK, London WC2A 3PX, England, UK

Signaling microclusters are a common feature of lymphocyte activation. However, the mechanisms controlling the size and organization of these discrete structures are poorly understood. The Ezrin-Radixin-Moesin (ERM) proteins, which link plasma membrane proteins with the actin cytoskeleton and regulate the steady-state diffusion dynamics of the B cell receptor (BCR), are transiently dephosphorylated upon antigen receptor stimulation. In this study, we show that the ERM proteins ezrin and moesin influence the organization and integrity of BCR microclusters. BCR-driven inactivation of ERM proteins is accompanied by a temporary increase in BCR diffusion, followed by BCR immobilization. Disruption of ERM protein function using dominant-negative or constitutively active ezrin constructs or knockdown of ezrin and moesin expression quantitatively and qualitatively alters BCR microcluster formation, antigen aggregation, and downstream BCR signal transduction. Chemical inhibition of actin polymerization also altered the structure and integrity of BCR microclusters. Together, these findings highlight a crucial role for the cortical actin cytoskeleton during B cell spreading and microcluster formation and function.

CORRESPONDENCE
Facundo D. Batista:
facundo.batista@cancer.org.uk
OR
Bebhinn Treanor:
bebhinn.treanor@cancer.org.uk

Abbreviations used: AU, arbitrary units; ERK, extracellular signal-regulated kinase; ERM, Ezrin-Radixin-Moesin; F-actin, filamentous actin; Hel, hen egg lysozyme; IRM, interference reflection microscopy; shRNA, short hairpin RNA; siRNA, small interfering RNA; TIRF, total internal reflection fluorescence; TIRFM, TIRF microscopy.

The sensing of extracellular stimuli enables cells to respond to changing circumstances for adaptation and survival. This is mediated by cell surface receptors, which upon binding ligand initiate a cascade of intracellular signaling, leading to alterations in gene expression. Commonly, the binding of ligands to such cell surface receptors leads to an alteration in the distribution of these receptors within the cell membrane. This redistribution of receptors may potentiate intracellular signaling by, for example, altering the localization of the receptor to kinase-rich membrane microdomains or facilitating the exclusion of phosphatases.

For B lymphocytes, an essential component of the adaptive immune system, specific recognition of foreign pathogens (antigen) by the BCR leads to the rapid formation of numerous small clusters of BCR and antigen (Depoil et al., 2008). These antigen receptor microclusters recruit several downstream signaling molecules and adaptors and are thus sites of active signaling (Depoil et al., 2008; Weber et al., 2008). We have previously shown that BCR recognition of antigen presented on the surface of other cells is accompanied a two-phase cellular response characterized by rapid spreading of the B cell over the antigen-bearing membrane, followed by a slower contraction phase (Fleire et al., 2006). During the spreading phase, numerous microclusters of BCR and antigen form throughout the contact site, which are then centrally aggregated during cell contraction. This spreading response is dependent on the affinity and density of antigen and requires both the initiation of intracellular signaling and reorganization of the actin cytoskeleton. Importantly, the number of microclusters formed during the spreading response determines the amount of antigen gathered for subsequent internalization for processing and presentation to T cells and thus the recruitment of T cell help, which is a critical component of B cell activation.

Interestingly, microclusters of antigen receptors and signaling molecules are formed upon recognition of antigen in both B cells and T cells (Bunnell et al., 2002; Campi et al., 2005;

The Rockefeller University Press $30.00
J. Exp. Med. Vol. 208 No. 5 1055-1068
www.jem.org/cgi/doi/10.1084/jem.20101125

The Journal of Experimental Medicine

Yokosuka et al., 2005; Depoil et al., 2008; Weber et al., 2008). These structurally discrete clusters appear to be a common feature of lymphocyte activation and thus may represent the basic unit of lymphocyte signaling. How these signaling microstructures are organized and maintained is an important question for understanding lymphocyte signaling and activation. Surprisingly, in both T cells and B cells, the diameter of a microcluster is ~300–600 nm, even across a 10-fold range of antigen densities (Bunnell et al., 2002; Campi et al., 2005; Yokosuka et al., 2005; Depoil et al., 2008). Moreover, each microcluster is initially spatially discrete, and fusion of clusters is only observed once microclusters have begun translocation toward the center of contact. These observations suggest that there is a mechanism that defines the size and spatial distribution of microclusters. However, what this mechanism is has yet to be resolved. What is clear is that microcluster formation is independent of immunoreceptor signaling, as indicated by microcluster formation in the presence of the Src family kinase inhibitor PP2 in T cells (Campi et al., 2005; Yokosuka et al., 2005) or signaling-deficient B cells (Depoil et al., 2008; Weber et al., 2008), although fewer microclusters are formed under these conditions. In contrast, pretreatment of T cells with actin-depolymerizing agents abrogates microcluster formation (Campi et al., 2005; Yokosuka et al., 2005; Varma et al., 2006), indicating an essential role for the actin cytoskeleton in the initiation of microcluster formation. However, immunoreceptor stimulation also induces a rapid depolymerization of actin followed by repolymerization (Hao and August, 2005; Ilani et al., 2007), suggesting that reorganization of the actin cytoskeleton is an important step in lymphocyte activation.

Moreover, both TCR and BCR stimulation induce a transient dephosphorylation of Ezrin-Radixin-Moesin (ERM) proteins (Delon et al., 2001; Faure et al., 2004; Gupta et al., 2006; Ilani et al., 2007), which are a family of highly conserved proteins that provide a regulated linkage between integral plasma membrane proteins and the actin cytoskeleton. Phosphorylation of a conserved threonine in the cytoplasmic tail induces a conformational opening of the protein to expose a FERM domain in the N terminus and an actin-binding domain in the C terminus (Bretscher et al., 2002). Thus, these proteins could provide a mechanism to rapidly alter the interaction between the plasma membrane and the underlying actin cytoskeleton upon antigen receptor stimulation and thus may be an important component of a network that regulates antigen receptor microclusters. Indeed, we have recently demonstrated that an ezrin- and actin-defined network regulated the steady-state diffusion dynamics of the BCR (Treanor et al., 2010). However, the role of this network during BCR microcluster formation has not been examined. In this study, we show that BCR signaling induces a transient localized dephosphorylation of ERM proteins. This transient inactivation of ERM proteins is accompanied by an initial increase in the diffusion of unengaged BCRs, followed by receptor immobilization. Using chimeric mutated versions of ezrin, we show that this BCR-induced reorganization of the ERM network is necessary for B cell spreading and antigen aggregation. Using GFP-tagged ezrin to visualize this network, we show that the ERM network is rapidly reorganized to surround BCR-antigen microclusters. Importantly, we find that ezrin and moesin play redundant, but important roles in antigen aggregation and BCR microcluster formation. Thus, disruption of either the ERM or the actin network affects the organization and integrity of BCR-antigen microclusters and their coalescence within the immune synapse.

RESULTS

BCR signaling induces reorganization of ERM proteins and alteration of BCR diffusion dynamics

To investigate how BCR stimulation impacts the ERM network, we initially examined the phosphorylation of ERM proteins upon BCR stimulation by immunofluorescence and confocal microscopy. We incubated primary naive B cells on a surface coated with immobilized stimulatory antibodies for various times and then fixed and stained the cells for threonine phosphorylated ERM proteins. ERM proteins were rapidly dephosphorylated upon BCR stimulation, followed by rephosphorylation at later time points (Fig. 1, A and B), which is consistent with a previous biochemical study using soluble antigen stimulation (Gupta et al., 2006). Moreover, we observed that this dephosphorylation was localized to the stimulatory surface (unpublished data). Thus, to examine the localization of phosphorylated ERM proteins with respect to antigen microclusters, total internal reflection fluorescence (TIRF) microscopy (TIRFM) was combined with a glass-supported planar lipid bilayer system in which fluorescently labeled streptavidin was used to tether a monobiotinylated model antigen, hen egg lysozyme (Hel). Hel-specific transgenic primary naive B cells were settled on planar lipid bilayers containing antigen for 90 s and then fixed and stained for phosphorylated ERM proteins. Puncta of phosphorylated ERM proteins that were located adjacent to BCR microclusters were often observed in primary naive mouse B cells (Fig. 1 C, top row). In contrast, in naive B cells deficient in key BCR signaling molecules such as PLCγ2 and Vav1/2, spatially distinct puncta of phosphorylated ERM proteins were not readily observed but instead appeared more clustered and frequently colocalized with BCR microclusters (Fig. 1 C, middle and bottom rows). Indeed, measurement of colocalization between phosphorylated ERM and BCR showed a higher degree of colocalization, particularly in Vav1/2-KO B cells (Fig. 1 D). Moreover, the mean intensity of phosphorylated ERM proteins at the contact site was increased in both PLCγ2- and Vav1/2-deficient B cells (Fig. 1 E), indicating that BCR signaling triggers a dephosphorylation and reorganization of the ERM network.

We have previously shown that in unstimulated B cells, the ERM network restricts BCR dynamics by defining diffusion boundaries (Treanor et al., 2010). Thus, we were keen to assess whether the dephosphorylation of ERM proteins upon BCR stimulation would affect BCR dynamics. We tracked single molecules of the BCR in unstimulated cells and upon stimulation with immobilized antigen at very early time points

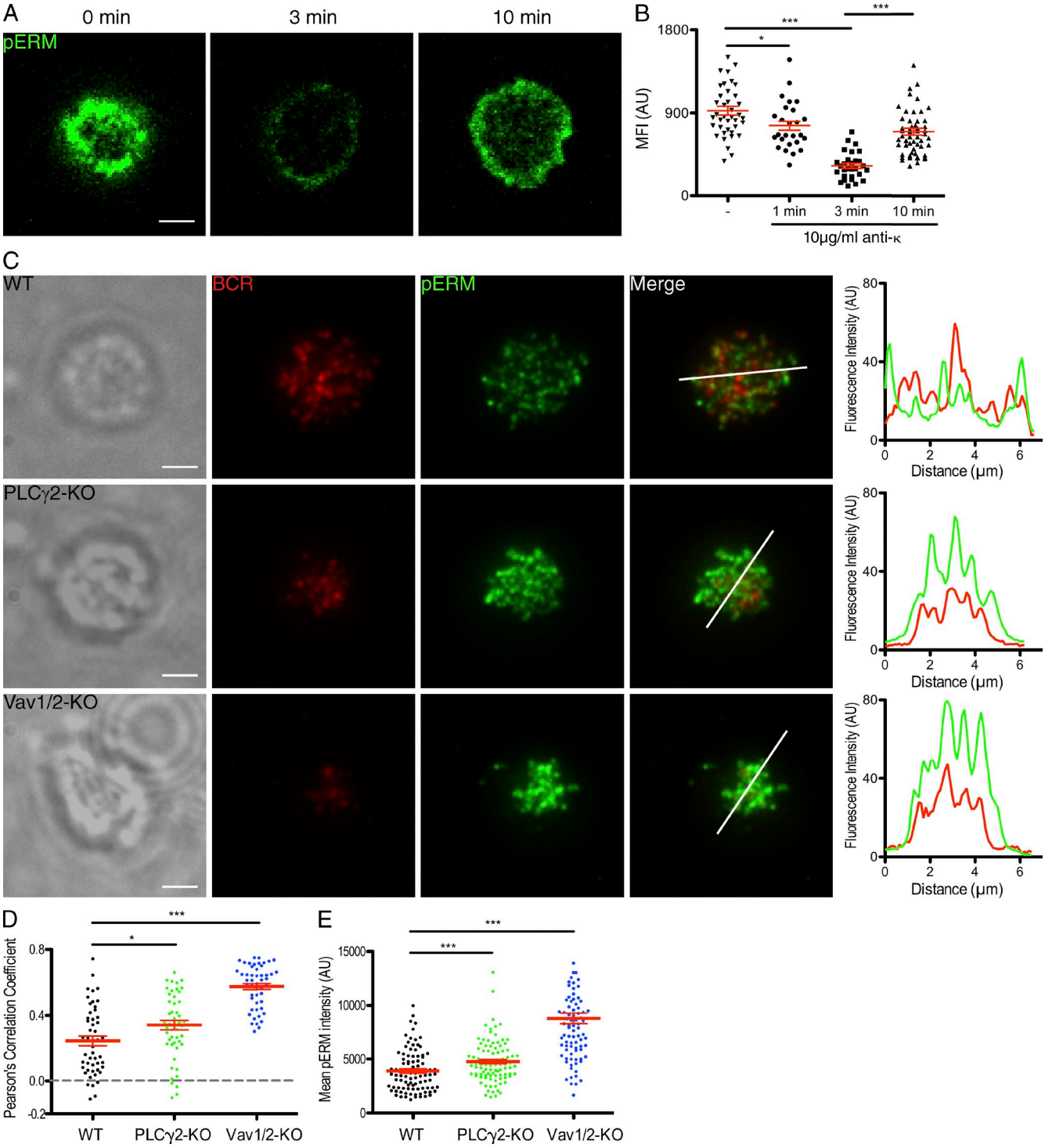

Figure 1. BCR signaling induces transient dephosphorylation of ERM proteins. (A and B) Primary WT splenic B cells were incubated on glass slides coated or not with 10 µg/ml anti-κ antibody for the indicated periods of time and then fixed and stained for threonine phosphorylation of ERM proteins (pERM) and imaged by confocal microscopy. (A) Representative image. (B) Quantification of the change in mean fluorescence intensity (MFI) of pERM in individual cells over time upon stimulation. Red bars indicate mean ± SEM. *, P = 0.0198; ***, P < 0.0001. (C–E) Primary WT (C, top), PLCγ2-KO (C, middle), or Vav1/2-KO (C, bottom) B cells labeled with Cy3 anti-IgM Fab were fixed on antigen-containing lipid bilayers after 1.5 min of interaction for subsequent pERM immunofluorescence and imaged by TIRFM. (C, left) Representative images. (right) Fluorescence intensity profile of BCR and pERM along the white lines. (D) Quantification of the segregation of BCR and pERM fluorescence in individual cells using Pearson's correlation coefficient, with the mean ± SEM indicated by the red bars. *, P = 0.0211; ***, P < 0.0001. (E) Quantification of mean pERM fluorescence intensity at the cell–bilayer contact, with the mean ± SEM indicated by the red bars. ***, P = 0.0008 (PLCγ2-KO); ***, P < 0.0001 (Vav1/2-KO). Data are representative of two independent experiments. Bars, 2 µm.

after cell contact and at later time points. A low number of BCRs (~1:500) on the cell surface of Hel-specific B cells expressing GFP-tagged ezrin were labeled with fluorescently labeled anti-IgM–specific Fab fragments and imaged by Dual View TIRFM as previously described (Treanor et al., 2010). Consistent with our previous study, the BCR displayed both immobile and mobile behaviors with a median diffusion coefficient of 0.033 μm s^{-1} in unstimulated cells (Fig. 2, A and B). At later time points after antigen stimulation, an increased number of BCRs became immobilized, and as a result, there was a reduction in the median diffusion coefficient (0.023 μm s^{-1}; Fig. 2, A–C). This would be consistent with the formation of BCR microclusters (Depoil et al., 2008), which has been recently suggested to depend on the Cμ4 domain of membrane Ig (Tolar et al., 2009). However, not all IgM molecules became immobilized, suggesting that only a proportion of the total BCRs on the cell surface are present within microclusters. Interestingly, a transient increase in BCR diffusion was observed at early time points upon antigen stimulation (0–5 min), with the median diffusion coefficient increasing to 0.047 μm s^{-1} (Fig. 2, A and B), reflecting a reduction in the proportion of very slow diffusing BCR (Fig. 2 C).

To determine whether these BCR dynamics reflected that of unengaged BCRs, we took advantage of the fact that these cells express both Hel-specific IgM as well as an endogenous IgG. This therefore allowed us to track single molecules of unengaged IgM upon stimulation of IgG. Importantly, a similar transient increase in diffusion of IgM was observed after stimulation of IgG (Fig. 2, D and E). These results are consistent with BCR signaling–induced inactivation of ERM proteins leading to a transient increase in the diffusion of neighboring unengaged BCRs. Moreover, a small proportion of IgM was also immobilized at later time points, suggesting that a degree of unengaged receptors are also immobilized after BCR stimulation.

Reorganization of ERM proteins is necessary for B cell spreading and antigen aggregation

If BCR signaling regulates the ERM-mediated interaction between the plasma membrane and the actin cytoskeleton, what happens if we prevent BCR-induced ERM reorganization? To examine the potential role of ERM proteins, we have used GFP-tagged WT ezrin (Ezrin-WT) and two chimeras, one with a point mutation of the putative activation-dependent phosphorylation residue, rendering it constitutively active (Ezrin-CA), and a truncated version that lacks the actin-binding domain

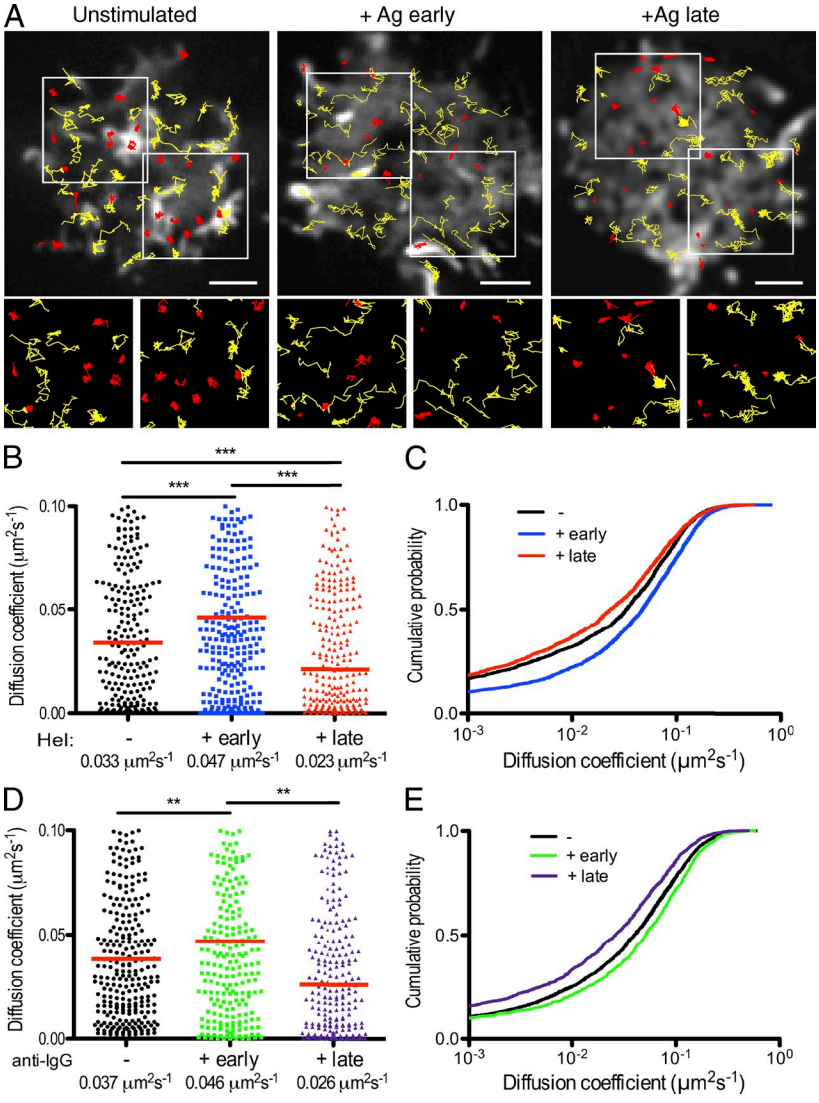

Figure 2. BCR signaling induces a transient increase in BCR diffusion followed by receptor immobilization. (A) Dual View TIRFM to simultaneously visualize ezrin-GFP (grayscale) and track single molecules of IgM in Hel-specific A20 B cells either unstimulated or during early (<5 min) and later (>15 min) times after settling on Hel-coated coverslips. Tracks are color-coded based on their diffusion coefficient to highlight slow diffusing IgM: red < 0.01 μm^2 s^{-1} and yellow > 0.01 μm^2 s^{-1}. Images in the bottom row are the zoomed regions indicated by white boxes. Ag, antigen. Bars, 2 μm. (B) Diffusion coefficients of single molecules of IgM in unstimulated and at early (<5 min) and late (>15 min) time points after stimulation with immobilized Hel, with the median indicated under the x axis and by the red bars. ***, P < 0.0001. (C) Cumulative probability plots for the data shown in B, in which a shift to the right or the left indicates increased and decreased diffusion, respectively. (D) Diffusion coefficients of single molecules of IgM in Hel-specific A20 B cells either unstimulated or at early (<5 min) and late (>15 min) time points after stimulation with anti-IgG, with the median indicated under the x axis and by the red bars. **, P = 0.0012. (E) Cumulative probability plots for the data shown in E. Data are representative of at least two independent experiments.

(Ezrin-DN), acting as a dominant-negative for both ezrin and moesin (Fig. 3 A). We took advantage of the DT40 chicken B cell line as the dynamics of BCR are similar to that observed in primary naive B cells (Treanor et al., 2010). Consistent with previous studies of ezrin localization in other cell types (Bretscher et al., 2002), Ezrin-WT was localized to intracellular regions as well as the plasma membrane, including cell surface membrane protrusions such as microvilli (Fig. 3 B, left).

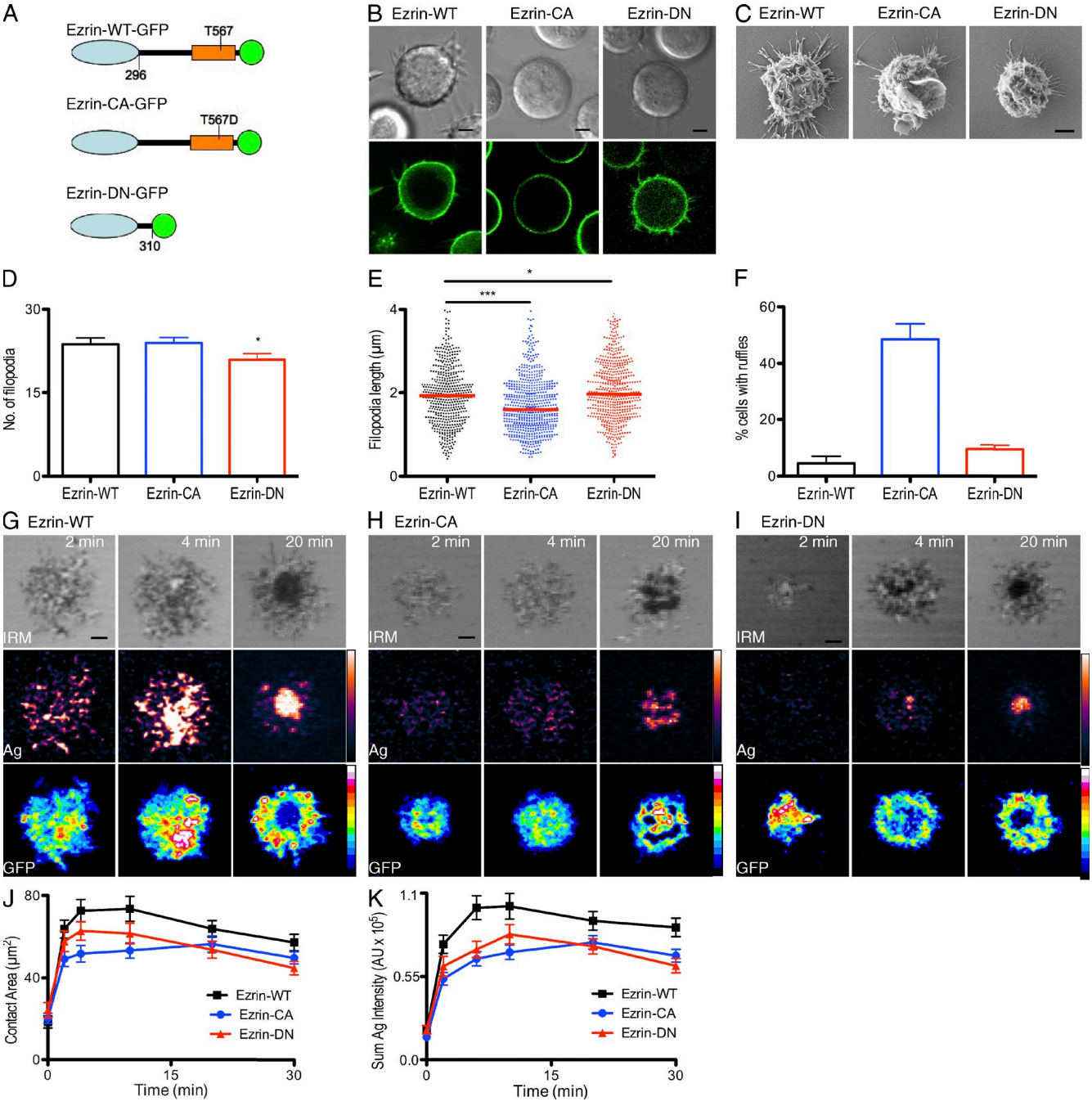

Figure 3. Disruption of ERM function impairs B cell spreading and antigen aggregation. (A) Schematic of GFP-tagged ezrin constructs. (B) Localization of GFP-tagged WT and mutated versions of ezrin were visualized by confocal microscopy in unstimulated DT40 B cells. (C) Scanning electron microscopy images of DT40 B cells expressing WT and mutated versions of ezrin after settling onto planar lipid bilayers containing anti-IgM as antigen. (D–F) Individual cells were quantified for the number of filopodia (D; *, P = 0.047), length of filopodia (E; *, P = 0.0369; ***, P < 0.0001), and frequency of cells with ruffles (F). (E) Red bars indicate mean. (G–I) DT40 B cells expressing WT Ezrin-GFP (G), Ezrin-CA–GFP (H), and Ezrin-DN–GFP (I) were settled onto lipid bilayers containing anti-IgM. Contact area was visualized by IRM (top), and fluorescently labeled antigen (Ag; middle) and GFP-tagged ezrin (bottom) were visualized by confocal microscopy at the indicated times. Antigen and GFP are mapped to a pseudocolor scale to aid visualization. (J and K) Contact area (J) and total antigen intensity within the contact area (K) were quantified over time. Data are representative of at least two independent experiments. (D, F, J, and K) Error bars indicate SEM. Bars, 2 µm.

Importantly, stable expression of Ezrin-WT did not dramatically alter cell morphology compared with untransfected cells (unpublished data). In contrast, Ezrin-CA was predominantly localized to the plasma membrane and was frequently observed polarized to one side of the cell (Fig. 3 B, middle). Ezrin-DN, which cannot bind actin but can still bind to integral membrane proteins, was localized to the plasma membrane including microvilli (Fig. 3 B, right). To further examine the morphology of these cells, we visualized B cells expressing these ezrin chimeras by scanning electron microscopy (Fig. 3 C). In contrast to cells expressing Ezrin-WT, which show cell surface microvilli and filopodia, cells expressing Ezrin-CA had shorter filopodia projections and frequently displayed large ruffles on the dorsal cell surface (Fig. 3, D–F). In contrast, B cells expressing Ezrin-DN had slightly fewer and longer filopodia compared with Ezrin-WT cells (Fig. 3, D and E). These observations suggest that simply altering the interaction between the plasma membrane and the actin cytoskeleton is sufficient to alter morphological features, which may impair B cell spreading and antigen aggregation.

To investigate this possibility, we visualized B cells spreading on antigen containing lipid bilayers by confocal fluorescence microscopy and interference reflection microscopy (IRM). IRM images clearly showed that B cells expressing Ezrin-WT were able to spread and contract in response to membrane-bound antigen (Fig. 3 G, top row), in a similar manner to that observed for WT B cells (Weber et al., 2008). Small clusters of antigen formed during the spreading phase and then were centrally aggregated into a single large cluster, from which GFP-tagged ezrin was excluded (Fig. 3 G, middle and bottom rows). In contrast, B cells expressing Ezrin-CA were impaired in their ability to spread, suggesting that alteration of cellular cortical tension is an important step to permit morphological changes during cell spreading (Faure et al., 2004). Moreover, instead of the central accumulation of antigen observed in WT cells, ezrin was not effectively excluded from the central region, as we observed exclusion in only 28% (±4%) of the cells compared with 67% (±4%) of Ezrin-WT–expressing cells (Fig. 3 H and not depicted). However, we also find that expression of Ezrin-DN, which presumably reduces cellular cortical tension (Faure et al., 2004), also impaired B cell spreading (Fig. 3 I). These results suggest that the ERM-mediated connection between the actin cytoskeleton and the plasma membrane is also important for cell spreading, which is consistent with active ERM proteins localizing to cell surface protrusions, including filopodia (Nakamura et al., 2000). Most strikingly, clusters of antigen were difficult to observe by confocal microscopy, and the central accumulation of antigen was reduced (Fig. 3 I). The area of spreading was reduced by ∼30% and 20% in B cells expressing Ezrin-CA and Ezrin-DN, respectively (Fig. 3 J). In addition, the total antigen intensity was reduced by a third in cells expressing either Ezrin-CA or Ezrin-DN compared with Ezrin-WT cells (Fig. 3 K). These results indicate that disruption of ezrin function alters the interaction of the actin cytoskeleton with the plasma membrane and thus disrupts B cell spreading and antigen aggregation.

The ERM network corrals BCR microclusters

Our observation of impaired antigen aggregation in cells expressing mutated forms of ezrin suggests that the ERM network is dynamically reorganized during microcluster formation. To investigate this, B cells expressing Ezrin-WT were settled onto planar lipid bilayers containing antigen and visualized at high resolution by TIRFM (Fig. 4 A and Video 1). We observed that during the initial stages of microcluster formation, ezrin was enriched and colocalized with developing clusters. However, as the fluorescence intensity of microclusters increased, the fluorescence intensity of ezrin diminished from the site of the microcluster, which is consistent with an initial dephosphorylation, and then reorganized around the antigen microcluster. These observations suggest that BCR signaling within developing microclusters leads to the localized reorganization of the ezrin network. This corralling of antigen microclusters may function to organize and provide structural integrity to these discrete clusters.

If this were the case, we would expect to observe defects in the organization and integrity of antigen microclusters when we disrupt ERM function. Indeed, in contrast to cells expressing Ezrin-WT, in which spatially discrete antigen microclusters of similar size and fluorescence intensity were observed, larger aggregates of antigen with increased fluorescence intensity were observed in cells expressing Ezrin-CA (Fig. 4, B–D). However, the mean number of antigen microclusters (37 ± 3 compared with 57 ± 4) was also markedly reduced in these cells, and as a result, the total antigen intensity at the contact was reduced by 50% (Fig. 4, E and F), which is consistent with the defect in cell spreading shown in Fig. 3. In contrast, small ill-defined antigen microclusters were observed in cells expressing Ezrin-DN (Fig. 4, B–D). Indeed, the mean intensity of antigen microclusters was less than half that of cells expressing Ezrin-WT (Fig. 4 C). The reduced fluorescence intensity of many of the microclusters observed in these cells did not fulfill the threshold for bona fide microclusters based on WT cells, and as a result, the total number of antigen microclusters was also decreased (34 ± 5; Fig. 4 E). Consequently, the total antigen intensity was reduced nearly fivefold compared with Ezrin-WT cells (Fig. 4 F). These results indicate that the ERM network serves to define the integrity of antigen microclusters. This process of B cell spreading and microcluster formation is critical to efficiently elicit downstream signaling and B cell activation (Fleire et al., 2006; Depoil et al., 2008). Indeed, we found that extracellular signal-regulated kinase (ERK) phosphorylation was reduced in B cells expressing either Ezrin-CA or Ezrin-DN, with a 50% reduction in phosphorylation of ERK at early time points (Fig. 4, G–J). In addition, cells expressing Ezrin-DN had markedly reduced sustained ERK phosphorylation compared with cells expressing Ezrin-WT (Fig. 4, H and J). It may be that there is a preexisting defect in signaling molecules as a result of the altered membrane organization; however, we were unable to detect alterations in steady-state signaling in these cells (unpublished data). Thus, the results presented here indicate that the corralling of BCR microclusters by the

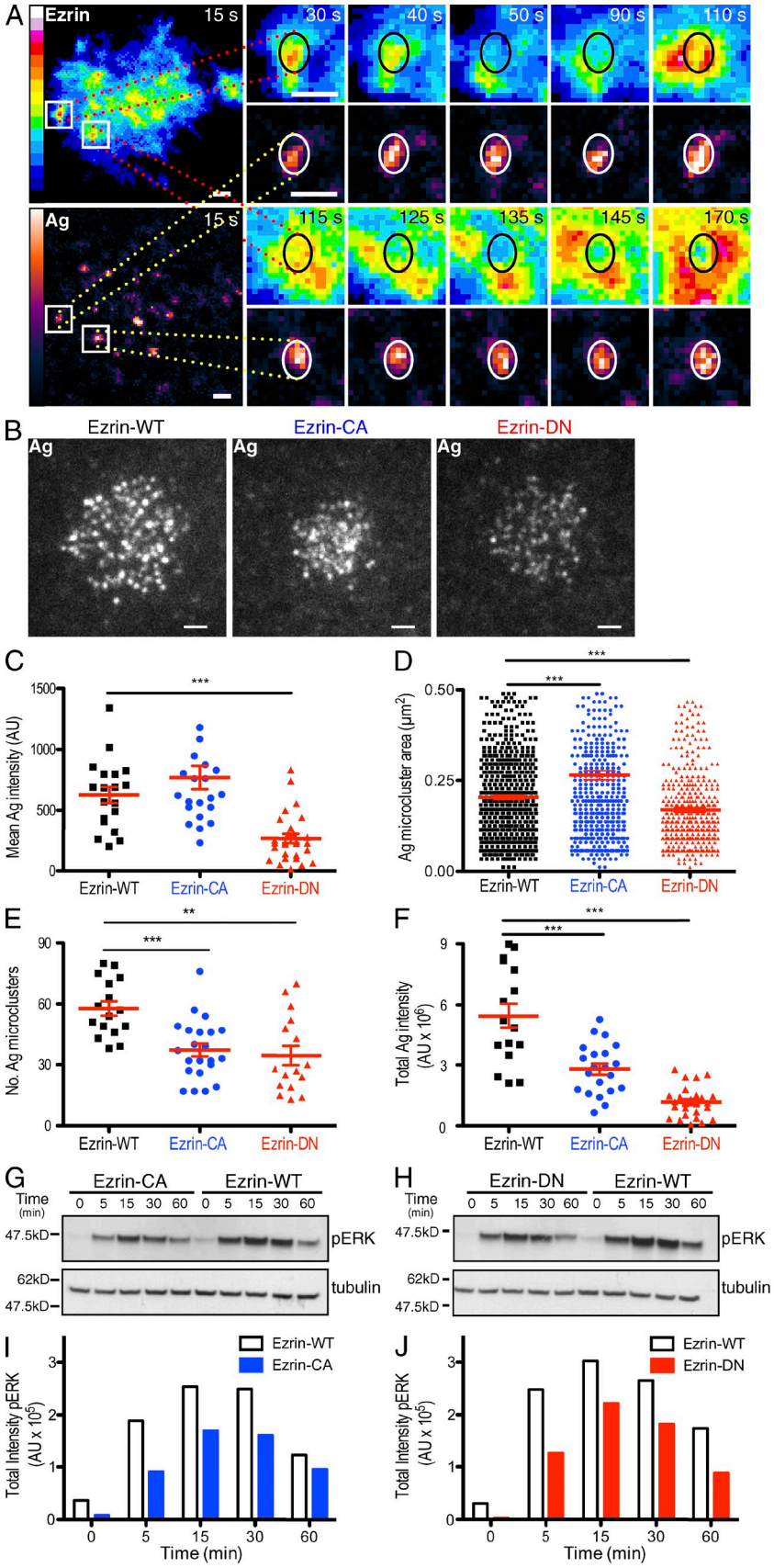

Figure 4. Dynamic reorganization of the ERM network is important for microcluster formation. (A) DT40 B cells expressing Ezrin-WT–GFP were settled onto planar lipid bilayers containing antigen (Ag) and visualized by TIRFM. GFP and antigen images are pseudocolored according to the lookup tables on the left. Images in the right panels are magnified time sequence images of the left panel (boxed areas) highlighting regions of ezrin (dotted red lines) and antigen (dotted yellow lines). White ovals indicate antigen microcluster and corresponding location with respect to ezrin (black ovals). (B) Representative images of antigen microclusters in DT40 B cells expressing Ezrin-WT, Ezrin-CA, or Ezrin-DN on planar lipid bilayers. (C) Quantification of the mean intensity of antigen microclusters in cells expressing Ezrin-WT (625.4 ± 66.2 arbitrary units [AU]), Ezrin-CA (769.1 ± 37.9 AU), and Ezrin-DN (267.2 ± 95.9 AU). ***, $P < 0.001$. (D) Quantification of the area of antigen microclusters in cells expressing Ezrin-WT (0.204 ± 0.006 µm), Ezrin-CA (0.265 ± 0.013 µm), and Ezrin-DN (0.017 ± 0.006 µm). ***, $P = 0.0004$. (E) Quantification of the number of antigen microclusters in cells expressing Ezrin-WT (58 ± 3), Ezrin-CA (37 ± 3), and Ezrin-DN (34 ± 5). **, $P = 0.002$; ***, $P = 0.0003$. (F) Quantification of the total antigen intensity at the contact in cells expressing Ezrin-WT ($5.4 \times 10^6 \pm 6.1 \times 10^5$ AU), Ezrin-CA ($2.8 \times 10^6 \pm 2.7 \times 10^5$ AU), and Ezrin-DN ($1.2 \times 10^6 \pm 1.5 \times 10^5$ AU). ***, $P < 0.0001$. Data are representative of at least two experiments with the mean ± SEM indicated in red. Between 16 and 28 cells were quantified in each cell type, representing a total of 2,298 microclusters. (G and H) Cells expressing WT and mutated ezrin were settled onto anti-IgM–coated plates for the indicated time. Cells were lysed and analyzed by SDS-PAGE followed by immunoblotting with anti–phospho-p44 and -p42 MAPK (Erk1 and Erk2) or antitubulin. (I and J) Comparison of the normalized intensity of pERK upon stimulation in cells expressing Ezrin-CA–GFP (I) or Ezrin-DN–GFP (J) with WT Ezrin-GFP. Data are representative of at least two independent experiments. Bars, 2 µm.

ERM network is important for the stability of BCR microclusters and consequently downstream signaling.

To dissect the contribution of the ERM proteins expressed in B cells, ezrin and moesin, we have taken an RNA interference approach (Fig. 5 A). Knockdown of either ezrin or moesin alone does not affect antigen aggregation or BCR microcluster formation (Fig. 5, B–F). However, knockdown of both ezrin and moesin resulted in a decrease in both the area of antigen aggregation and the total antigen intensity after 10 min of interaction with planar lipid bilayers containing antigen (Fig. 5, B–D). Moreover, we also found that knockdown of both ezrin and

moesin affects the number of BCR microclusters (Fig. 5, E and F), and consequently reduces downstream signaling upon BCR stimulation with membrane-bound antigen (Fig. 5 G). These results are consistent with disruption of ERM function using dominant-negative ezrin. Collectively, these results indicate that ezrin and moesin play a redundant, but significant role in microcluster formation and antigen aggregation in B cells, which is consistent with ezrin and moesin functioning together to promote T cell activation (Shaffer et al., 2009).

The ERM network regulates the translocation and fusion of microclusters

As the ERM network surrounds individual microclusters (Fig. 4 A), we would expect that this network must be reorganized to allow microcluster fusion and translocation. Consistent with our previous observations, antigen microclusters were localized to regions of reduced ezrin intensity but were tightly enclosed by higher intensity Ezrin-GFP (Fig. 6 A and Video 2). Notably, we observed that during translocation to the center, the ezrin network appeared to dynamically gate microcluster movement and fusion, that is, the ezrin network surrounding each microcluster appeared to disassemble and reassemble to permit microcluster fusion into larger clusters (Fig. 6 A and Video 3). In contrast, in cells expressing Ezrin-CA, the ERM network was not tightly

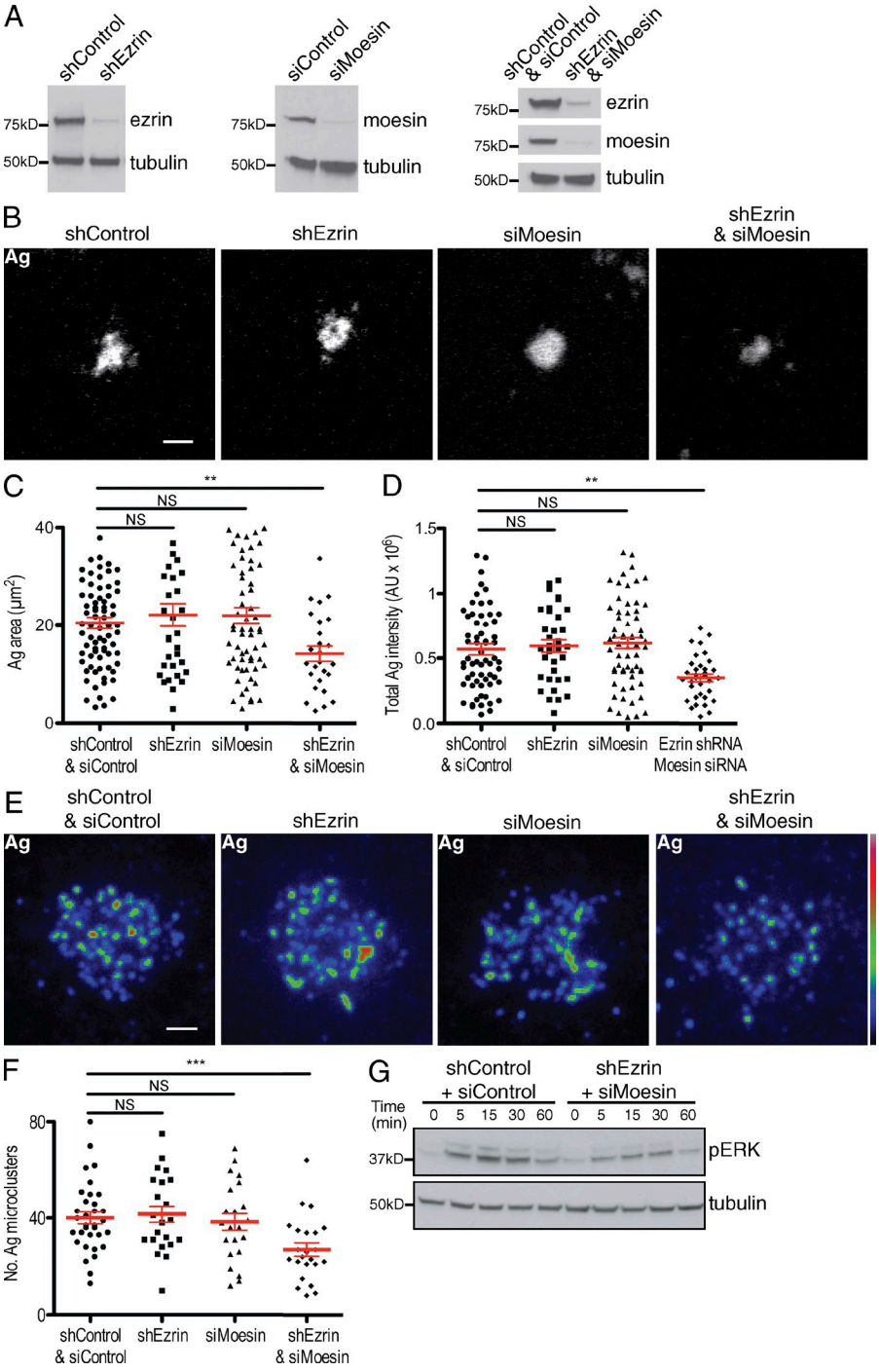

Figure 5. Knockdown of both ezrin and moesin impairs microcluster formation and antigen aggregation. (A) Hel-IgM A20 B cells stably expressing control or ezrin shRNA (left), transiently transfected with control or moesin siRNA (middle), or stably expressing control or ezrin shRNA and then transiently transfected with control or moesin siRNA (right) were lysed and analyzed by SDS-PAGE followed by immunoblotting with anti-ezrin, antimoesin, and antitubulin as indicated. (B–D) Hel-IgM A20 B cells expressing control shRNA, ezrin shRNA, moesin siRNA, or ezrin shRNA and moesin siRNA were settled onto lipid bilayers containing Hel as antigen (Ag). (B) Fluorescently labeled antigen was visualized by confocal microscopy after 10 min of interaction. (C and D) Contact area (C; **, P = 0.0047) and total antigen intensity within the contact area (D; **, P = 0.0018) were quantified after 10 min of interaction in individual cells. (E) Representative images of antigen microclusters in A20 B cells expressing control shRNA and control siRNA, ezrin shRNA, moesin siRNA, or ezrin shRNA and moesin siRNA on planar lipid bilayers. (F) Quantification of the number of antigen microclusters in cells expressing control shRNA and control siRNA (40 ± 3), ezrin shRNA (42 ± 3), moesin siRNA (38 ± 3), and ezrin shRNA and moesin siRNA (27 ± 3). ***, P = 0.0007. (G) Cells expressing control shRNA and control siRNA or ezrin shRNA and moesin siRNA were settled onto anti-IgM–coated plates for the indicated time. Cells were lysed and analyzed by SDS-PAGE followed by immunoblotting with anti–phospho-p44 and -p42 MAPK (Erk1 and Erk2) or antitubulin. Data are representative of at least two independent experiments. (C, D, and F) Error bars indicate mean ± SEM. Bars, 2 μm.

organized around these clusters, and as a result, antigen microclusters were larger and not spatially discrete (Fig. 6 B and Videos 4 and 5), which is consistent with our previous observations (Fig. 4, B and D). Conversely, there was no clear localization of Ezrin-DN and antigen microclusters; however, microclusters were rapidly transported to the center of contact and rarely fused during translocation (Fig. 6 C and Videos 6 and 7). These observations are consistent with this ezrin mutant essentially being a membrane-associated protein that cannot exert its actin-binding function.

Given that we observed dynamic ERM-mediated gating of microclusters during translocation, we next tracked the movement of antigen microclusters in cells in which ezrin function was altered. In cells expressing Ezrin-WT, antigen microclusters translocated from the periphery of cell contact toward the center in relatively straight lines, with some tracks showing evidence of jostling and temporary confinement (Fig. 6 D). The median diffusion coefficient of these antigen microclusters was 4.2×10^{-4} μm s^{-1} (Fig. 6 E). In cells expressing Ezrin-DN, antigen microclusters readily translocated from the periphery to the center of contact in nearly straight tracks at a rate similar to that observed in WT cells (Fig. 6, D–F). In contrast, tracking of antigen microclusters in cells expressing Ezrin-CA showed increased confinement and few microclusters translocated to the center (Fig. 6 D). Consistent with these observations, the median diffusion coefficient was 7.4×10^{-5} μm s^{-1}, a fivefold reduction compared with Ezrin-WT cells (Fig. 6 E). This reduction in diffusion represented a marked increase in the frequency of very slow moving microclusters (Fig. 6 F). These results indicate that remodeling of the ERM network is necessary for the dynamic translocation and fusion of microclusters in the center of contact.

The structure, organization, and integrity of signaling microclusters is dependent on the actin cytoskeleton

Our data have demonstrated an important role for the ERM network in the organization and integrity of BCR-antigen microclusters. This crucial role for the ERM network is likely the result of its interaction with the underlying actin cytoskeleton, which provides the structural scaffold for BCR microcluster organization and stability. Thus, we would predict that if we disassemble the underlying actin cytoskeleton, we would disrupt BCR microclusters. However, as cell spreading and microcluster formation is abrogated if cells are pretreated with actin-depolymerizing agents (Campi et al., 2005; Yokosuka et al., 2005; Fleire et al., 2006), B cells expressing the kinase Syk-GFP were allowed to spread and form microclusters before the actin-depolymerizing agent, Latrunculin A, was injected into the imaging chamber. Depolymerization of actin caused the rapid arrest of antigen microcluster translocation toward the center (Video 8), which is consistent with TCR microcluster translocation (Varma et al., 2006). Moreover, we observed that depolymerization of filamentous actin (F-actin) also led to an alteration in both the size and fluorescence intensity of antigen and Syk-containing microclusters (Fig. 7 and Video 8). Indeed, we observed a nearly 50% decrease in the fluorescence intensity of both antigen and Syk-containing microclusters within 10 min of treatment (Fig. 7 B and not depicted). Moreover, we observed that actin disruption caused the dispersion of antigen and Syk clusters into less well-defined clusters, which in some instances appeared to break up and then fuse with neighboring clusters (Video 8). As a result, the mean size of microclusters increased twofold (Fig. 7 C). An interesting question is whether the sensitivity of the BCR to actin disruption is dependent on antigen affinity. However, these data clearly indicate that the actin cytoskeleton acts as an important scaffold for defining the organization, size, and integrity of signaling microclusters in B cells.

DISCUSSION

Collectively, the results presented in this study are consistent with the following model of BCR-induced cytoskeleton remodeling upon antigen stimulation. BCR signaling upon antigen engagement triggers a localized dephosphorylation of ERM proteins and thus the dissociation of the plasma membrane from the underlying actin cytoskeleton. This inactivation of ERM proteins and detachment of the actin cytoskeleton, as well as perhaps the initial depolymerization of F-actin upon BCR stimulation as previously reported (Hao and August, 2005; Gupta et al., 2006), lead to a loss of BCR diffusion barriers (Treanor et al., 2010) and thus to a transient increase in diffusion of unengaged BCRs. Intriguingly, we have previously reported that BCR signaling is positively correlated with increased BCR diffusion (Treanor et al., 2010). Thus, opening up of the ERM and actin-defined diffusion barrier might be an important step that increases the diffusion of unengaged BCRs, which might then join a newly forming microcluster and/or permit association with critical coreceptors.

ERM inactivation is also important for B cell spreading over the antigen-containing membrane, which is consistent with ERM proteins mediating cytoskeleton relaxation and promoting T cell antigen–presenting cell conjugation (Faure et al., 2004). Moreover, our data indicate an important role for ERM proteins in the driving mechanism of B cell spreading as cells expressing Ezrin-DN exhibited defects in cell spreading. Because we know that B cell spreading is actin dependent (Fleire et al., 2006), it may be that by coupling actin to the plasma membrane, ERM proteins are important for F-actin organization and lamellipodium formation, as suggested in other cell types (Baumgartner et al., 2006). In line with this, ezrin accumulates in F-actin–rich membrane protrusions at the periphery of the immunological synapse in T cells (Roumier et al., 2001). More recently, defects in cell spreading upon ezrin silencing in T cells have been attributed to disorganization of the microtubule network (Lasserre et al., 2010), although it remains to be determined whether this also occurs in B cells.

Importantly, our results also indicate that ERM reorganization is necessary for antigen aggregation. Although some of the observed defects in antigen aggregation are caused by the defect in cell spreading, particularly in the case of cells expressing Ezrin-CA, the defect in antigen aggregation in cells expressing Ezrin-DN cannot be attributed solely to diminished cell

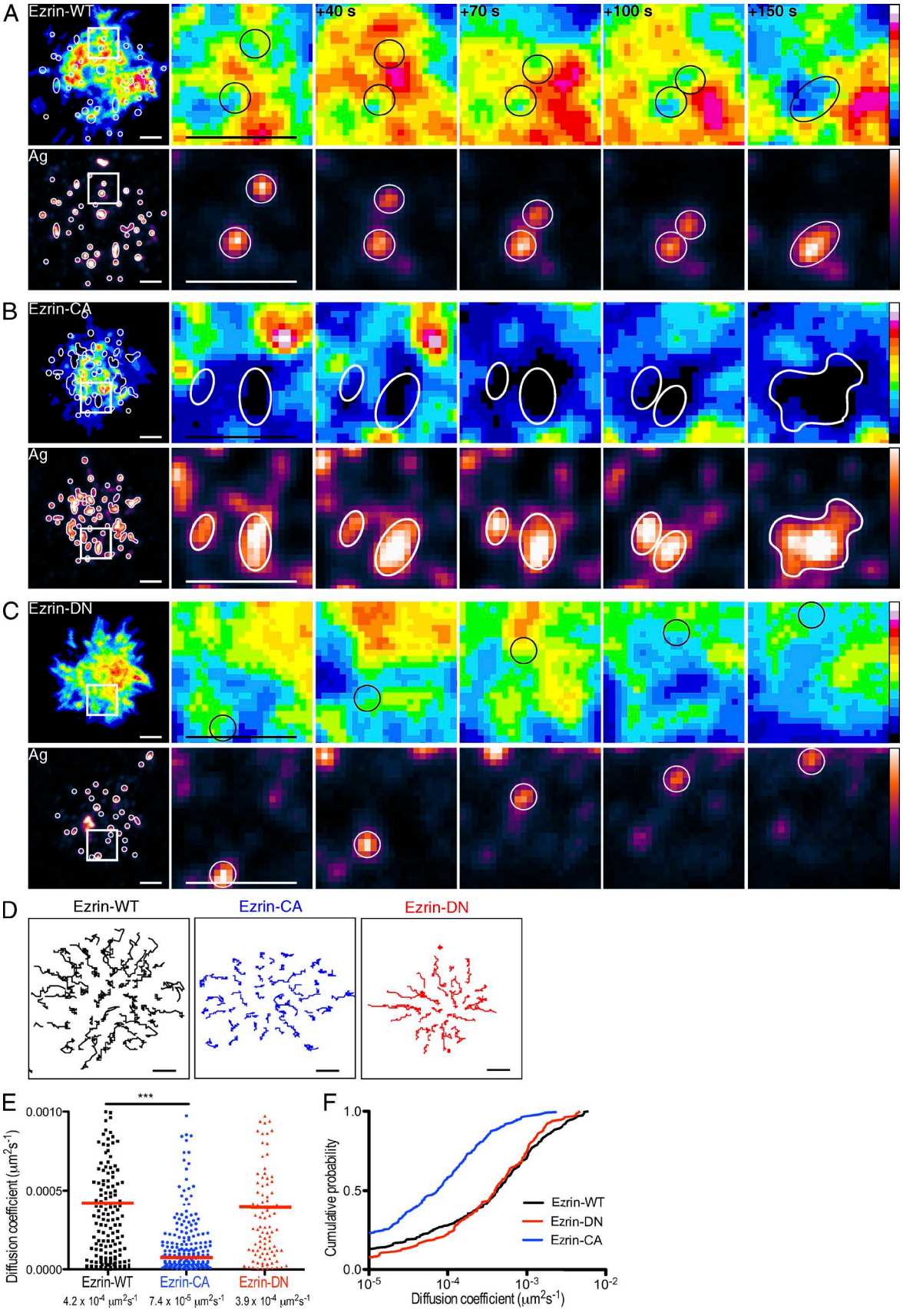
A
Ezrin-WT
+40 s
+70 s
+100 s
+150 s
Ag
B
Ezrin-CA
Ag
C
Ezrin-DN
Ag
D
Ezrin-WT
Ezrin-CA
Ezrin-DN
E
***
0.0010
0.0005
0.0000
Diffusion coefficient (μm²s⁻¹)
Ezrin-WT
Ezrin-CA
Ezrin-DN
4.2 x 10⁻⁴ μm²s⁻¹
7.4 x 10⁻⁵ μm²s⁻¹
3.9 x 10⁻⁴ μm²s⁻¹
F
1.0
0.5
0.0
Cumulative probability
Ezrin-WT
Ezrin-DN
Ezrin-CA
10⁻⁵
10⁻⁴
10⁻³
10⁻²
Diffusion coefficient (μm²s⁻¹)

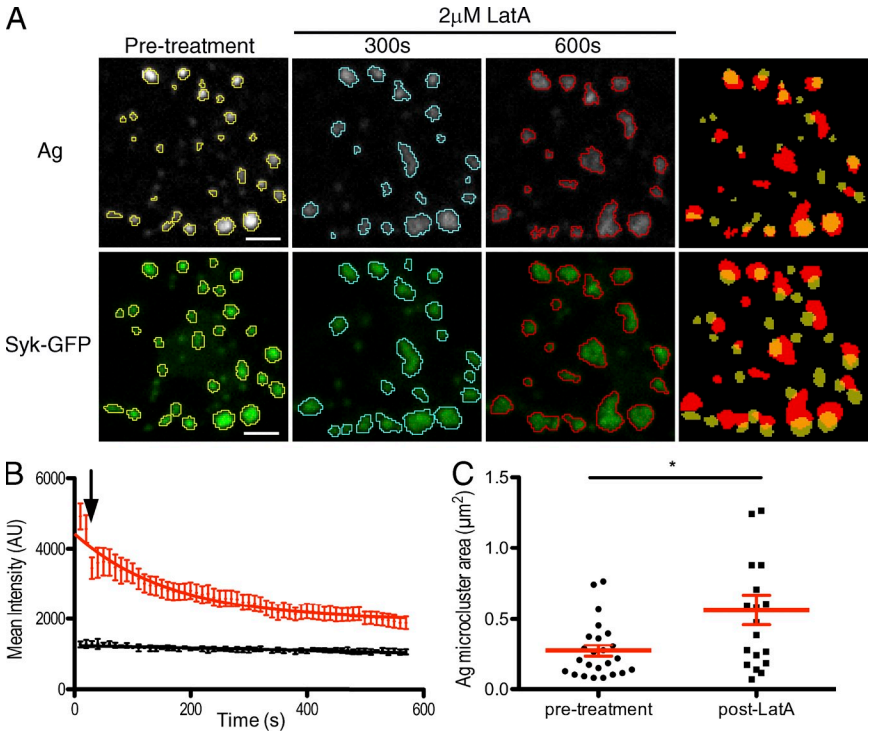

Figure 7. The actin cytoskeleton is important for the structure and integrity of signaling microclusters. (A) Hel-specific A20 B cells expressing GFP-Syk were settled on planar lipid bilayers containing antigen (Ag) and imaged by TIRFM. Cells were allowed to spread and form microclusters before 2 μM Latrunculin A (LatA) was injected into the imaging chamber. Cells were imaged every 10 s for 20 min. Antigen and GFP-Syk clusters before treatment (yellow outline), 300 s after treatment (blue outline), and 600 s after treatment (red outline) are shown. Overlaid images of microclusters before Latrunculin A treatment (filled yellow) and 600 s after treatment (filled red) are shown in the right column. (B) Mean intensity ± SEM of antigen microclusters (red line) was quantified over time after injection of 2 μM Latrunculin A (indicated by black arrow). Background control (black line) indicates negligible photobleaching over the image acquisition. (C) Antigen microcluster area was measured before (circles) and 600 s after 2 μM Latrunculin A (squares) with the mean ± SEM indicated in red. *, P = 0.02. Data are representative of at least two independent experiments.

spreading as the mean intensity of microclusters was markedly reduced. Instead, our results suggest that rephosphorylation of ERM proteins mediate assembly of a plasma membrane–bound actin network, which forms an enclosure or corral around individual microclusters. Interestingly, a recent study suggested that antigen engagement induces a conformational change in the Fc portion of the BCR to reveal an interface in the Cμ4 domain that promotes BCR oligomerization and clustering (Tolar et al., 2009). However, our data suggest an additional layer of regulation mediated by the cortical actin cytoskeleton, which is important for the organization and stability of microclusters. Our data show that depolymerization of actin by treatment with Latrunculin A results in the disassembly of microclusters, indicating that protein–protein interactions alone are not sufficient to support microcluster stability. It may also be that ERM-defined actin corrals create diffusion barriers that trap unengaged receptors within microclusters. In line with this, we observed that upon stimulation of IgG, a small proportion of IgM became immobilized, suggesting that a degree of unengaged receptors are also immobilized after BCR stimulation. However, it remains to be determined whether this is caused by immobilization within antigen receptor microclusters. This is an important question as it is currently not clear whether BCRs and antigen are present in a one to one stoichiometry within microclusters or whether there is serial engagement of BCRs within microclusters.

The ERM network is then dynamically reorganized, undergoing local activated and deactivated states that permit the fusion and coalescence of microclusters as they translocate to the center of contact. Our observation that Ezrin-DN does not affect microcluster translocation rates suggests that the ERM network itself is not involved in the driving mechanism of microcluster translocation, which may be driven by actomyosin contractility (Salaita et al., 2010) or retrograde actin flow, as suggested for other receptor complexes (Lidke et al., 2005). However, increased barriers created by constitutively active ezrin hindered microcluster movement, indicating that remodeling of the ERM network is necessary for the dynamic translocation and fusion of microclusters in the center of contact. Interestingly, these data are consistent with recent work in which the speed of microcluster translocation was reduced by chromium-defined substrate constraints (DeMond et al., 2008). Moreover, a recent study in human breast cancer cells has shown that nanopatterned grid barriers that restrict the

Figure 6. Microcluster fusion and dynamics depend on ERM remodeling. (A–C) DT40 B cells expressing Ezrin-WT (A), Ezrin-CA (B), or Ezrin-DN (C) were settled onto planar lipid bilayers containing antigen (Ag) and visualized by TIRFM. GFP and antigen images are pseudocolored according to the lookup tables on the right. Images in the right panels are magnified time sequence images of the left panel (boxed areas). White ovals indicate antigen microcluster and corresponding location with respect to ezrin (black ovals). (D–F) Antigen microclusters were tracked in cells expressing Ezrin-WT, Ezrin-CA, and Ezrin-DN. (D) Representative examples of microcluster tracks during cell contraction. (E and F) Diffusion coefficients with the median indicated under the x axis and by the red bars (E) and cumulative probability plots of antigen microclusters (F). ***, P < 0.0001. Data are representative of at least two independent experiments. Bars, 2 μm.

radial transport of EphA2 receptors alter microcluster organization and, consequently, the cellular response to ephrin-A1, suggesting a spatio-mechanical regulation of EphA2 signaling (Salaita et al., 2010). Importantly, receptor–ligand organization and radial transport was strongly correlated with invasion potential. Interestingly, this study implicated the ezrin-binding membrane–bound glycoprotein CD44 in EphA2 receptor reorganization. If we consider this in the context that several studies have implicated ezrin in tumor invasion and metastasis (Hunter, 2004; Khanna et al., 2004; Yu et al., 2004), it may be that ERM-defined physical barriers act as spatio-mechanical regulators of receptor signaling.

Collectively, our data provide evidence that ERM proteins act as an integral component of an actin-dependent structural scaffold, which defines the organization and integrity of antigen microclusters. By taking an RNA interference approach, we have found that the ERM proteins expressed in B cells, ezrin and moesin, play a redundant role in these processes, which is consistent with ezrin and moesin functioning together to promote T cell activation (Shaffer et al., 2009). It may also be that additional proteins, which form part of the structural scaffold linking the plasma membrane to the actin cytoskeleton, such as spectrin, ankyrin, and protein 4.1, may also be important regulators of plasma membrane organization and compartmentalization of cell surface proteins. The ERM proteins may only be one part of the picture, but as the activation state of ERM proteins is modified by immunoreceptor signaling, it provides an elegant mechanism to dynamically regulate interactions between the actin cytoskeleton and the plasma membrane to tune both diffusion dynamics at the level of single molecules as well as the fusion and translocation of macromolecular complexes.

MATERIALS AND METHODS

Cell preparation and culture. C57BL/6 WT mice, *Plcγ2*$^{fl/fl}$ *Cd19*Cre$^{+/-}$ mice (Hashimoto et al., 2000) provided by T. Kurosaki (Institute of Physical and Chemical Research, Yokohama, Japan), and *Vav1*$^{-/-}$*Vav2*$^{-/-}$ (Doody et al., 2001) provided by M. Turner (Babraham Institute, Cambridge, England, UK) were used. Splenic naive B cells were purified as described previously (Carrasco et al., 2004). This purification resulted in a population with 95–98% B cells. Primary B cells and A20 B cells expressing Hel-specific IgM (Williams et al., 1994) were cultured in RPMI 1640 containing 10% FCS, penicillin and streptomycin antibiotics (Invitrogen), and 50 µM 2-mercaptoethanol (Sigma-Aldrich). DT40 B cells were cultured at 39.5°C in RPMI 1640 containing 10% FCS, 1% chicken serum, penicillin and streptomycin antibiotics, and 50 µM 2-mercaptoethanol. All experiments were approved by the Cancer Research UK Animal Ethics Committee and the UK Home Office.

Short hairpin RNA (shRNA)– and small interfering RNA (siRNA)–mediated knockdown. Hel-IgM A20 B cells were infected with control shRNA or ezrin shRNA lentiviral particles (SMARTvector 2.0; Thermo Fisher Scientific) in the presence of 10 µg/ml polybrene, and stable cells were selected with 4 µg/ml puromycin. Hel-IgM A20 B cells and control shRNA or ezrin shRNA stables were transiently transfected (Nucleofector; Lonza) with 1 µM control or moesin siRNA and analyzed 48 h later. Knockdown of ezrin and moesin was assessed by Western blot using antiezrin- and antimoesin-specific antibodies (Cell Signaling Technology).

Reagents. 2 µM Latrunculin A (EMD) prewarmed in PBS was injected into FCS2 chambers during imaging. Ezrin-GFP, Ezrin-CA–GFP, and Ezrin-DN–GFP constructs were gifts from E. Sahai (London Research Institute, Cancer Research UK, London, England, UK; Sahai and Marshall, 2003).

Glass coverslip coating. Acid-cleaned glass coverslips were incubated with 4 µg/ml fibronectin (Sigma-Aldrich) for 1 h or 5 µg/ml anti-IgM or IgG for 3 h at 37°C and washed with PBS.

Planar lipid bilayers. Planar lipid bilayers containing ICAM-1 at ∼70 molecules/µm^2 and different ligands at 75 molecules/µm^2 were prepared in FCS2 chambers (Bioptechs) by liposome spreading as previously described (Carrasco et al., 2004). In brief, Alexa Fluor 633 streptavidin (Invitrogen) was incorporated into lipid bilayers to which monobiotinylated antigens, including Hel and anti–chicken IgM, were tethered. Assays were performed in chamber buffer (0.5% FCS, 2 mM Mg^{2+}, 0.5 mM Ca^{2+}, and 1 g/liter D-glucose in PBS) at 37°C.

Immunostaining. Primary naive mouse B cells were settled on anti-IgM–coated coverslips or planar lipid bilayers containing Hel as antigen for the indicated time and then fixed with 4% paraformaldehyde for 10 min at 37°C. Cells were permeabilized with 0.1% Triton X-100/PBS for 5 min at room temperature, blocked with 5% goat serum/0.1% Triton X-100/PBS for 1 h at room temperature, and then incubated overnight with anti–phospho-Ezrin (Thr567)/Radixin (Thr564)/Moesin (Thr558; Cell Signaling Technology), followed by incubation with Alexa Fluor 488–conjugated Fab_2 goat anti–rabbit IgG (H+L; Invitrogen).

Cell labeling for single particle tracking. A20 B cells were labeled with Cy3-labeled goat anti–mouse IgM Fab fragment (Jackson ImmunoResearch Laboratories, Inc.). B cells were incubated with 1 ng/ml labeled anti-IgM mixed with 2 µg/ml unlabeled anti-IgM Fab (Jackson ImmunoResearch Laboratories, Inc.) in chamber buffer for 15 min at 4°C and then washed with PBS.

Cell stimulation and immunoblotting. DT40 B cells stably expressing WT ezrin-GFP, Ezrin-CA–GFP, or Ezrin-DN–GFP were equilibrated in RPMI at 37°C for 10 min and plated onto immobilized stimulatory anti-IgM (clone M4) for the indicated time. Cells were lysed in 2× Laemmli sample buffer and analyzed by SDS-PAGE, followed by immunoblotting with anti–phospho-p44 and -p42 MAPK (Erk1 and Erk2) or anti-p44 and -p42 MAPK (Cell Signaling Technology).

Statistical analysis. Cumulative probability plots and the nonparametric Wilcoxon Mann-Whitney test were performed on data using Prism version 5.00 for Windows (GraphPad Software).

Microscopy. Confocal fluorescence, differential interference contrast, and IRM images were acquired with an Axiovert LSM 510 (Carl Zeiss). For scanning electron microscopy images, cells were fixed on lipid bilayers with 2.5% gluteraldehyde/4% paraformaldehyde and processed as previously described (Fleire et al., 2006). TIRF images and single molecule fluorescence microscopy were performed using a TIRFM system based on an inverted microscope (IX81; Olympus), 150× NA 1.45 TIRFM objective (Olympus), motorized filter wheel (Olympus), sensitive electron-multiplying charge-coupled device camera (Cascade II; Photometrics), and real-time data acquisition (Cell^R; Olympus). Three laser lines (488, 561, and 635 nm) can be used simultaneously while TIRF illumination is individually adjusted using three separate TIRFM illumination combiners (Olympus). Simultaneous two-channel recording was accomplished by mounting an image splitter (Optosplit II; Cairn Research) and a second electron-multiplying charge-coupled device camera (Quant EM 512SC; Photometrics) on the bottom port. Image acquisition for the second camera was recorded with Image-Pro Plus (Media Cybernetics). Image registration was achieved by measuring the position of fluorescent microspheres (TetraSpek 0.1 µm; Invitrogen).

Image processing. The contact area of the B cell with the antigen-containing lipid bilayer, the amount and area of aggregated antigen, and Pearson's

Correlation coefficients were quantified using Volocity (PerkinElmer). The enrichment of antigen and phosphorylated ERM proteins was determined using the plot profile function in ImageJ (National Institutes of Health). Antigen and GFP images were pseudocolored using the gem and 16-color lookup table provided in ImageJ, respectively. Dual View TIRFM channels of ezrin and BCR were split using the Cairn Image Splitter plugin of ImageJ. Ezrin images were background subtracted (rolling ball size 30) and Gaussian filtered (sigma radius 1) using ImageJ.

Single molecule detection. Single molecule imaging was performed as previously described (Treanor et al., 2010). In brief, an area of ~2,300 μm^2 was illuminated by 3.5-mW laser power, resulting in a power density of ~150 W/cm^2 out of the objective. Frame rates of 20 frames/s were used to record image sequences of 200 frames. The signal to noise ratio, defined as the peak intensity after background subtraction divided by the standard deviation of the background fluctuations, was measured on one experimental dataset as 7.2 ± 0.6 ($n = 10$; Bobroff, 1986).

Online supplemental material. Video 1 shows the organization of GFP-tagged ezrin in relation to antigen microclusters visualized by TIRFM. Videos 2–7 show the fusion and dynamics of antigen microclusters in B cells expressing Ezrin-WT, Ezrin-CA, and Ezrin-DN visualized by TIRFM. Video 8 shows the effect of Latrunculin A treatment on antigen and Syk-containing microclusters over time as visualized by TIRFM. Online supplemental material is available at http://www.jem.org/cgi/content/full/jem.20101125/DC1.

We would like to thank Michele Weber for the data in Fig. 1 A and for help with EM images together with Hannah Armer and Lucy Collinson. We thank T. Kurosaki for PLCγ2-deficient mice and M. Turner for Vav1 and Vav2 double-deficient mice. We would also like to thank members of the Lymphocyte Interaction Laboratory for critically reading the manuscript and for helpful discussions.

This work was supported by Cancer Research UK and the Royal Society Wolfson Research Merit Award (to F.D. Batista).

The authors declare that they have no competing financial interests.

Submitted: 7 June 2010
Accepted: 9 March 2011

REFERENCES

Baumgartner, M., A.L. Sillman, E.M. Blackwood, J. Srivastava, N. Madson, J.W. Schilling, J.H. Wright, and D.L. Barber. 2006. The Nck-interacting kinase phosphorylates ERM proteins for formation of lamellipodium by growth factors. *Proc. Natl. Acad. Sci. USA*. 103:13391–13396. doi:10.1073/pnas.0605950103

Bobroff, N. 1986. Position measurement with a resolution and noise-limited instrument. *Rev. Sci. Instrum.* 57:1152–1157. doi:10.1063/1.1138619

Bretscher, A., K. Edwards, and R.G. Fehon. 2002. ERM proteins and merlin: integrators at the cell cortex. *Nat. Rev. Mol. Cell Biol.* 3:586–599. doi:10.1038/nrm882

Bunnell, S.C., D.I. Hong, J.R. Kardon, T. Yamazaki, C.J. McGlade, V.A. Barr, and L.E. Samelson. 2002. T cell receptor ligation induces the formation of dynamically regulated signaling assemblies. *J. Cell Biol.* 158:1263–1275. doi:10.1083/jcb.200203043

Campi, G., R. Varma, and M.L. Dustin. 2005. Actin and agonist MHC–peptide complex–dependent T cell receptor microclusters as scaffolds for signaling. *J. Exp. Med.* 202:1031–1036. doi:10.1084/jem.20051182

Carrasco, Y.R., S.J. Fleire, T. Cameron, M.L. Dustin, and F.D. Batista. 2004. LFA-1/ICAM-1 interaction lowers the threshold of B cell activation by facilitating B cell adhesion and synapse formation. *Immunity*. 20:589–599. doi:10.1016/S1074-7613(04)00105-0

Delon, J., K. Kaibuchi, and R.N. Germain. 2001. Exclusion of CD43 from the immunological synapse is mediated by phosphorylation-regulated relocation of the cytoskeletal adaptor moesin. *Immunity*. 15:691–701. doi:10.1016/S1074-7613(01)00231-X

DeMond, A.L., K.D. Mossman, T. Starr, M.L. Dustin, and J.T. Groves. 2008. T cell receptor microcluster transport through molecular mazes reveals mechanism of translocation. *Biophys. J.* 94:3286–3292. doi:10.1529/biophysj.107.119099

Depoil, D., S. Fleire, B.L. Treanor, M. Weber, N.E. Harwood, K.L. Marchbank, V.L. Tybulewicz, and F.D. Batista. 2008. CD19 is essential for B cell activation by promoting B cell receptor-antigen microcluster formation in response to membrane-bound ligand. *Nat. Immunol.* 9:63–72. doi:10.1038/ni1547

Doody, G.M., S.E. Bell, E. Vigorito, E. Clayton, S. McAdam, R. Tooze, C. Fernandez, I.J. Lee, and M. Turner. 2001. Signal transduction through Vav-2 participates in humoral immune responses and B cell maturation. *Nat. Immunol.* 2:542–547. doi:10.1038/88748

Faure, S., L.I. Salazar-Fontana, M. Semichon, V.L. Tybulewicz, G. Bismuth, A. Trautmann, R.N. Germain, and J. Delon. 2004. ERM proteins regulate cytoskeleton relaxation promoting T cell-APC conjugation. *Nat. Immunol.* 5:272–279. doi:10.1038/ni1039

Fleire, S.J., J.P. Goldman, Y.R. Carrasco, M. Weber, D. Bray, and F.D. Batista. 2006. B cell ligand discrimination through a spreading and contraction response. *Science*. 312:738–741. doi:10.1126/science.1123940

Gupta, N., B. Wollscheid, J.D. Watts, B. Scheer, R. Aebersold, and A.L. DeFranco. 2006. Quantitative proteomic analysis of B cell lipid rafts reveals that ezrin regulates antigen receptor-mediated lipid raft dynamics. *Nat. Immunol.* 7:625–633. doi:10.1038/ni1337

Hao, S., and A. August. 2005. Actin depolymerization transduces the strength of B-cell receptor stimulation. *Mol. Biol. Cell*. 16:2275–2284. doi:10.1091/mbc.E04-10-0881

Hashimoto, A., K. Takeda, M. Inaba, M. Sekimata, T. Kaisho, S. Ikehara, Y. Homma, S. Akira, and T. Kurosaki. 2000. Cutting edge: essential role of phospholipase C-gamma 2 in B cell development and function. *J. Immunol.* 165:1738–1742.

Hunter, K.W. 2004. Ezrin, a key component in tumor metastasis. *Trends Mol. Med.* 10:201–204. doi:10.1016/j.molmed.2004.03.001

Ilani, T., C. Khanna, M. Zhou, T.D. Veenstra, and A. Bretscher. 2007. Immune synapse formation requires ZAP-70 recruitment by ezrin and CD43 removal by moesin. *J. Cell Biol.* 179:733–746. doi:10.1083/jcb.200707199

Khanna, C., X. Wan, S. Bose, R. Cassaday, O. Olomu, A. Mendoza, C. Yeung, R. Gorlick, S.M. Hewitt, and L.J. Helman. 2004. The membrane-cytoskeleton linker ezrin is necessary for osteosarcoma metastasis. *Nat. Med.* 10:182–186. doi:10.1038/nm982

Lasserre, R., S. Charrin, C. Cuche, A. Danckaert, M.I. Thoulouze, F. de Chaumont, T. Duong, N. Perrault, N. Varin-Blank, J.C. Olivo-Marin, et al. 2010. Ezrin tunes T-cell activation by controlling Dlg1 and microtubule positioning at the immunological synapse. *EMBO J.* 29:2301–2314. doi:10.1038/emboj.2010.127

Lidke, D.S., K.A. Lidke, B. Rieger, T.M. Jovin, and D.J. Arndt-Jovin. 2005. Reaching out for signals: filopodia sense EGF and respond by directed retrograde transport of activated receptors. *J. Cell Biol.* 170:619–626. doi:10.1083/jcb.200503140

Nakamura, N., N. Oshiro, Y. Fukata, M. Amano, M. Fukata, S. Kuroda, Y. Matsuura, T. Leung, L. Lim, and K. Kaibuchi. 2000. Phosphorylation of ERM proteins at filopodia induced by Cdc42. *Genes Cells*. 5:571–581. doi:10.1046/j.1365-2443.2000.00348.x

Roumier, A., J.C. Olivo-Marin, M. Arpin, F. Michel, M. Martin, P. Mangeat, O. Acuto, A. Dautry-Varsat, and A. Alcover. 2001. The membrane-microfilament linker ezrin is involved in the formation of the immunological synapse and in T cell activation. *Immunity*. 15:715–728. doi:10.1016/S1074-7613(01)00225-4

Sahai, E., and C.J. Marshall. 2003. Differing modes of tumour cell invasion have distinct requirements for Rho/ROCK signalling and extracellular proteolysis. *Nat. Cell Biol.* 5:711–719. doi:10.1038/ncb1019

Salaita, K., P.M. Nair, R.S. Petit, R.M. Neve, D. Das, J.W. Gray, and J.T. Groves. 2010. Restriction of receptor movement alters cellular response: physical force sensing by EphA2. *Science*. 327:1380–1385. doi:10.1126/science.1181729

Shaffer, M.H., R.S. Dupree, P. Zhu, I. Saotome, R.F. Schmidt, A.I. McClatchey, B.D. Freedman, and J.K. Burkhardt. 2009. Ezrin and moesin function together to promote T cell activation. *J. Immunol.* 182:1021–1032.

Tolar, P., J. Hanna, P.D. Krueger, and S.K. Pierce. 2009. The constant region of the membrane immunoglobulin mediates B cell-receptor clustering and signaling in response to membrane antigens. *Immunity*. 30:44–55. doi:10.1016/j.immuni.2008.11.007

Treanor, B., D. Depoil, A. Gonzalez-Granja, P. Barral, M. Weber, O. Dushek, A. Bruckbauer, and F.D. Batista. 2010. The membrane skeleton controls diffusion dynamics and signaling through the B cell receptor. *Immunity*. 32:187–199. doi:10.1016/j.immuni.2009.12.005

Varma, R., G. Campi, T. Yokosuka, T. Saito, and M.L. Dustin. 2006. T cell receptor-proximal signals are sustained in peripheral microclusters and terminated in the central supramolecular activation cluster. *Immunity*. 25:117–127. doi:10.1016/j.immuni.2006.04.010

Weber, M., B. Treanor, D. Depoil, H. Shinohara, N.E. Harwood, M. Hikida, T. Kurosaki, and F.D. Batista. 2008. Phospholipase C-γ2 and Vav cooperate within signaling microclusters to propagate B cell spreading in response to membrane-bound antigen. *J. Exp. Med*. 205:853–868. doi:10.1084/jem.20072619

Williams, G.T., C.J. Peaker, K.J. Patel, and M.S. Neuberger. 1994. The alpha/beta sheath and its cytoplasmic tyrosines are required for signaling by the B-cell antigen receptor but not for capping or for serine/threonine-kinase recruitment. *Proc. Natl. Acad. Sci. USA*. 91:474–478. doi:10.1073/pnas.91.2.474

Yokosuka, T., K. Sakata-Sogawa, W. Kobayashi, M. Hiroshima, A. Hashimoto-Tane, M. Tokunaga, M.L. Dustin, and T. Saito. 2005. Newly generated T cell receptor microclusters initiate and sustain T cell activation by recruitment of Zap70 and SLP-76. *Nat. Immunol.* 6:1253–1262. doi:10.1038/ni1272

Yu, Y., J. Khan, C. Khanna, L. Helman, P.S. Meltzer, and G. Merlino. 2004. Expression profiling identifies the cytoskeletal organizer ezrin and the developmental homeoprotein Six-1 as key metastatic regulators. *Nat. Med*. 10:175–181. doi:10.1038/nm966